## Title

REACTION RATES OF HYDROXYL RADICAL WITH NITRIC ACID AND WITH HYDROGEN PEROXIDE



## Authors

Marinelli, W.J.
Johnston, H.S.

## Publication Date

1982-02-01

LBL-14293
Preprint

Lawrence Berkeley Laboratory
UNIVERSITY OF CALIFORNIA



Materials & Molecular
Research Division

Submitted to the Journal of Chemical Physics

# REACTION RATES OF HYDROXYL RADICAL WITH NITRIC ACID AND WITH HYDROGEN PEROXIDE

William J. Marinelli and Harold S. Johnston

February 1982



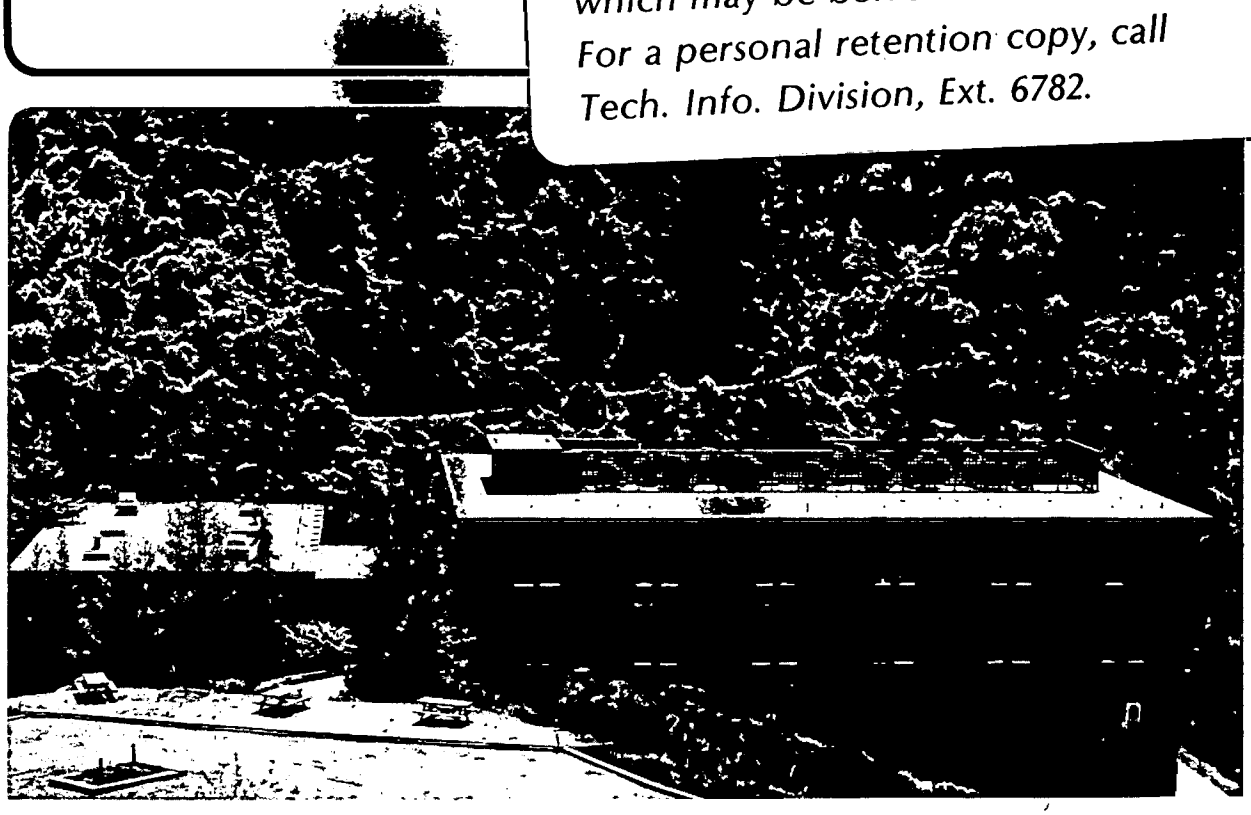

Prepared for the U.S. Department of Energy under Contract DE-AC03-76SF00098

## DISCLAIMER

# Reaction Rates of Hydroxyl Radical with Nitric Acid and with Hydrogen Peroxide

William J. Marinelli† and Harold S. Johnston

Department of Chemistry, University of California

and

Materials and Molecular Research Division

Lawrence Berkeley Laboratory

Berkeley, California 94720

## Abstract

The rates of the reactions

$$HO + HNO_3 \rightarrow H_2O + NO_3 \qquad (1)$$

$$HO + H_2O_2 \rightarrow H_2O + HOO \qquad (2)$$

have been studied by laser flash photolysis of reactants and resonance fluorescence of hydroxyl radicals. The recently reported high rate constants at room temperature for both reactions and the negative activation energy for (1) at low temperature have been confirmed. Results obtained here are: $k_1 = 1.52 \times 10^{-14} \exp(644/T)$ cm$^3$ molecule$^{-1}$ s$^{-1}$ from 218-363 K and $k_2 = 1.81 \times 10^{-12}$ cm$^3$ molecule$^{-1}$ s$^{-1}$ at 298 K. These two reactions have been examined by transition-state theory; (1) is assigned a cyclic and (2) a chain-like transition state. Even with no potential energy barrier, the reaction coordinate of (1) involves a quantum-mechanical, temperature independent frequency; and with this model the low pre-exponential factor and negative activation energy of reaction (1) can be explained.

This work was supported by the Director, Office of Energy Research, Office of Basic Energy Sciences, Chemical Sciences Division of the U.S. Department of Energy under Contrat No. DE-AC03-76SF00098.

†Present address: Department of Chemistry, Cornell University, Ithaca, New York 14853

## Introduction

Two recent measurements[1,2] of the rate coefficients for the reaction

$$HO + HNO_3 \rightarrow H_2O + NO_3 \qquad (1)$$

differ substantially from other measurements[3-6] both as to value at 298 K and as to temperature dependence. Wine et al.[1] found the second-order rate coefficient for (1) to be

$$k_1 = 1.52 \times 10^{-14} \exp(649/T) \text{ cm}^3 \text{ molecule}^{-1} \text{ s}^{-1}$$

over the temperature range 224-366 K. The reaction has a "negative activation energy," that is, the rate coefficient increases with a decrease in temperature.[1,2] The pre-exponential factor is about $10^{-14}$ $cm^3$ $molecule^{-1}$ $s^{-1}$, which appears to be low for a hydrogen-atom transfer reaction. It has been established that $NO_3$ is the primary product of this reaction.[6,7]

Also, recent measurements[8-11] find the rate coefficient for the reaction

$$HO + H_2O_2 \rightarrow H_2O + HOO \qquad (2)$$

to be faster than that indicated by earlier studies.[12-14] For example, Keyser[8] found the rate expression

$$k_2 = 2.15 \times 10^{-12} \exp(-126/T) \text{ cm}^3 \text{ molecule}^{-1} \text{ s}^{-1}$$

over the temperature range 245-423 K. The activation energy is of small magnitude but it has the usual sign, and the pre-exponential factor is within the range regarded as "normal."

Since recent measurements of the rate constants for reactions (1) and (2) differ substantially from the body of older data, it is desirable

to reinvestigate these reactions in several different laboratories. In the present study the technique of laser flash photolysis coupled with product detection by resonance fluorescence (FP/RF) was used to study reaction (1) from 218 to 363 K and to study reaction (2) at 298 K.

The ratio of pre-exponential factors for these two apparently similar reactions is 165, and the ratio of rate coefficients $k_2/k_1$ is 12 at room temperature. In view of the low pre-exponential factor for $k_1$, the negative activation energy for (1), and the large ratio $k_2/k_1$, a complex mechanism, such as

$$HO + HNO_3 \underset{M}{\overset{M}{\rightleftharpoons}} HO \cdot HNO_3 \xrightarrow{M} H_2O + NO_3 \qquad (3)$$

has been postulated where all steps presumably depend on foreign gas concentration. However, this study includes an examination of reactions (1) and (2) by simple activated complex theory,[15] in order to see if each of these reactions could be an elementary bimolecular reaction within the framework of this theory and with the values of $k_1$ and $k_2$ that have been recently obtained.

## Experimental

The apparatus used in these experiments is shown in Fig. 1. Two photolysis cells were employed. The first, designed after Magnotta,[16] was used for early experiments at 298 K. Later temperature-dependence experiments were performed in the cell shown in Fig. 2, similar to one described by Wine, Kreutter and Ravishankara.[17] The jacketed Pyrex

cell was externally blackened to reduce scattered light, wrapped with aluminum foil to minimize radiative heat exchange, and enclosed in a vacuum housing pumped to 10 microns for insulation. Methanol (218-273 K) or ethylene glycol (273-363 K) from a circulating temperature bath was passed through the cell jacket for temperature control. A temperature sensor, which could be inserted into the reaction zone, determined the gas temperature to ± 1 K. Two Suprasil-1 lenses were used weakly to focus light from the resonance lamp into the reaction zone and to collect resonantly scattered radiation for focusing on to the PMT detector. All window materials were Suprasil-1 or $CaF_2$.

The resonance lamp used for HO radical resonance fluorescence detection was operated with a 3% $H_2O$/Ar mixture at ∿ 700 microns total pressure, and used a 2.45 GHz current-stabilized microwave generator. Vycor was used as a lamp window to eliminate unwanted UV and VUV radiation emitted from the lamp. The detection system consisted of a cooled RCA 31034 PMT and a baffled Hoya "Peak 320" color filter and 307 ± 15 nm interference filter. These filters passed the HO ($A^2\Sigma^+ - X^2\pi_i$) (0,0) band while rejecting scattered photolysis laser light. Response of the detection system was shown to be linear from 0.5-5 x $10^{11}$ molecules/$cm^3$ with a sensitivity of 3 x $10^7$ molecules $cm^{-1}$ $Hz^{-1}$ by photolysis of a fixed $HNO_3$/Ar mixture at varying energies.

Hydroxyl radicals were produced by photolysis of the reactant molecules $HNO_3$ or $H_2O_2$. A Lumonics TE-860-2M rare gas halide excimer laser running on KrF at 248.4 nm and operated at 15 Hz with typical pulse energies of 10-20 mJ/$cm^2$ was used. Average laser power was measured using a Scientech surface absorbing power meter.

Concentrations of reactants were measured continuously using a UV absorption system. It consisted of a 1 meter long Pyrex cell, equipped with fused silica windows, through which the chopped output of a Beckman deuterium lamp was directed. Light emerging from the cell passed through a (McPherson 218) 0.3 meter monochrometer set at 0.3 nm bandpass and was detected by an RCA 1P28 photomultiplier coupled to a lock-in amplifier. The monitoring cell was run at ambient temperature. Readings from a second temperature sensor fixed to the cell were used to correct reactant concentrations for changes in gas density between the monitoring and photolysis cell due to temperature differences. Nitric acid and $H_2O_2$ were monitored at 200 nm using the absorption cross sections of Molina and Molina:[18] $\sigma_{HNO_3} = 6.6. \times 10^{-18}$ $cm^2$ $molecule^{-1}$ and $\sigma_{H_2O_2} = 4.67 \times 10^{-19}$ $cm^2$ $molecule^{-1}$. Reactants were introduced into the system via partial saturation of Ar carrier gas passed through a Pyrex saturator held at 232 or 244 K ($HNO_3$), or 273 K ($H_2O_2$). Fine control of reactant concentrations was accomplished using a split-flow system employing two Nupro type "s" stainless steel needle valves placed in the carrier gas lines before the saturator. The saturator was equipped with bypass valves which allowed only pure carrier gas to flow through the system and enabled the determination of the UV cell 100% transmission level. A short length of large diameter (1/2") tubing was used to connect the photolysis and monitoring cells, and a throttle valve was used to limit the pump-out rate of the system. Two cross-calibrated capacitance manometers placed at each end of the flow system showed less than a 1% pressure drop under flowing experimental conditions of 100 sccm Ar at 10 Torr total pressure. At higher pressures

a constant cell residence time was maintained by adjusting the flow rate and pump throttle valve. Under these conditions reactant concentrations were stable to within 3% after a 10 minute (600 residence times) equilibration period.

The PMT was operated in photon counting mode using a PAR 1121 amplifier/discriminator coupled to an SSR 1105 photon counter with an ECL/TTL converter and high speed line driver. Data were recorded using a Nicolet Instruments (Fabritek) 1074 instrument computer acting as a signal averager in multichannel scaling mode and analyzed using a PDP-8/L computer interfaced to the signal averager. Typically, 1024 channel segments at channel widths of 2-20 μs were used and 4096 or 8192 laser shots were averaged to obtain a first-order rate constant.

## Materials

The Ar (> 99.999%) and $N_2$ (> 99.998%) were supplied by Lawrence Berkeley Laboratory and used without further purification. Nitric acid was prepared by distillation from mixtures of $NaNO_3$ or $KNO_3$ in excess 96% $H_2SO_4$ under vacuum. The product was collected at 244 K (o-xylene slush) from a distillation flask held at 300 K with only the middle portion saved, and it was stored at 196 K. The concentration of $NO_2$ in the $HNO_3$ samples was always less than the detection limit of 0.05 percent. Hydrogen peroxide was purchased as a 90 or 98% solution from FMC Corporation and was degassed by pumping prior to use.

## Results

### The Reaction of HO with $HNO_3$

The FP/RF experiments were conducted under pseudo-first order conditions with reactant concentrations $10^2$-$10^4$ times greater than HO following the flash. The reaction of HO with $HNO_3$ was studied over a 23-fold range of $HNO_3$ concentration, a five-fold range of Ar carrier gas pressure from 10 to 50 Torr, and a 145 K temperature range from 218-363 K. The HO radical decays were analyzed using standard first-order techniques

$$\ell n\ F_t = \ell n\ F_o - k't \tag{4}$$

where F is the observed fluorescence signal which is proportional to the hydroxyl radical concentration

$$F = \alpha\ [HO] \tag{5}$$

so that (4) is equivalent to

$$\ell n\ [HO]_t = \ell n\ [HO]_o - k't \quad . \tag{6}$$

The pseudo-first order constant k' is determined by a least squares analysis of (4) or (6), and it has the property

$$k' = k_1\ [HNO_3] + k_d \quad . \tag{7}$$

The second-order rate constant of interest $k_1$ is obtained from the slope of a plot of k' vs $[HNO_3]$. The intercept gives $k_d$, which is a first-order rate constant describing HO removal processes not proportional to the concentration of reactant, such as diffusion, reaction with

carrier gas or impurities, and flow. In the $HNO_3$ study, corrections were considered for the competing reaction

$$HO + NO_2 \xrightarrow{M} HNO_3 \quad . \qquad (8)$$

The ratio of the rate of (8) to that of (1) is $k_8^o[M][NO_2]/k_1[HNO_3]$, where $k_8^o$ is the low-pressure limit, $2.6 \times 10^{-30}$ $(300/T)^5$. In all cases the ratio $[NO_2]/[HNO_3]$ was below the detection limit of $5 \times 10^{-4}$, and the maximum pressure was 50 Torr at room temperature and 25 Torr at other temperatures. The upper limit to the correction for (8) is 2% at 218 K, 1.5% at 300 K, and 0.5% at 363 K. Decays were typically followed for 1.5 to 3 hydroxyl radical lifetimes (1/e) with a return to baseline during the sweep in all but the lowest reactant concentration experiments. A typical HO radical decay is shown in Fig. 3 along with the least-squares fit to the data.

The pseudo-first order rate constants k' are plotted against the concentration of $HNO_3$ at 298 K for 10, 25, and 50 Torr of argon carrier gas in Fig. 4. The three lines are parallel to each other giving the same second-order rate coefficient, $k_1$. The intercepts are in the order one would expect from diffusion as the dominant effect in $k_d$: the largest $k_d$ is with 10 Torr carrier gas, the intermediate value is with 25 Torr, and the smallest value of $k_d$ is with 50 Torr. In the recent work by Nelson et al.,[6] the relation of $k_d$ to carrier gas pressure was in the inverse order, and one value of $k_d$ appeared to be unusually high. The current study involved many more rate-constant determinations, and the present results are regarded as more reliable than those of Nelson et al.[6] on this reaction. In addition, the rate constant was found to be independent of UV monitor location (before or

after the photolysis cell), linear flow rate through the reaction zone, and the type of photolysis cell. For a total of 61 first-order rate constants at 298 K, the average second-order rate constant ($\pm 2\sigma$) is $1.31 \pm 0.24 \times 10^{-13}$ $cm^3$ $molecule^{-1}$ $s^{-1}$. These results and the results at 218, 250, 273, 323, and 363 K are summarized in Table 1. An Arrhenius plot

$$k = A \exp(-E/RT) \tag{9}$$

for these results is shown in Fig. 5, and the temperature-dependent rate coefficient is $k_1 = (1.52 \pm 0.43) \times 10^{-14} \exp[(644 \pm 79)/T]$ $cm^3$ $molecule^{-1}$ $s^{-1}$. According to gas phase reaction rate theory, a low activation energy E may not be caused by a potential-energy barrier between reactants and products, but rather it may simply depend on the net power of T in the rate expression

$$k = BT^n \tag{10}$$

for which the "activation energy" is nRT. These data are plotted as log k vs log T in Fig. 6. The slope indicates the exponent n in (10) to be $-2.29 \pm 0.23$. Our results are compared with those of other investigators in Table 2. The results of this experiment are in very close agreement with those of Wine et al.[1] and in reasonably close agreement with those of Kurylo et al.[2]

## The Reaction of HO with $H_2O_2$

The hydrogen peroxide study covered a seven-fold range of reactant concentration at 298 K and 10 Torr argon pressure. Pseudo-first order rate constants are plotted against $H_2O_2$ concentrations in Fig. 7. This study covers a ten-fold range in initial HO concentration and includes 18 first-order rate constants. The value of the second-order rate

constant is $k_2 = (1.81 \pm 0.24) \times 10^{-12}$ cm$^3$ molecule$^{-1}$ s$^{-1}$. The result is compared with those of other investigators in Table 3. Within the cumulative error limits this result is in agreement with the four recent reports[8-11] that give $k_2 \pm 2\sigma$ of $(1.65 \pm 0.21) \times 10^{-12}$ cm$^3$ molecule$^{-1}$ s$^{-1}$ at 298 K.

## Discussion

### The Reaction of HO with $HNO_3$

The rate coefficient for the reaction of hydroxyl radicals with nitric acid has an exceptionally low pre-exponential factor and a negative activation energy, that is, the rate constant increases as the temperature decreases. One suggested explanation for these unusual features is that the process is chemically complex, consisting of two or more chemical reactions. The purpose of this section is to see if the results are — after all — quantitatively consistent with transition-state theory as applied to an elementary reaction.

Nitric acid is a planar molecule, where the hydrogen atom is hydrogen-bonded to an oxygen atom to make a four-member ring,[20] Fig. 8. The hydrogen atom undergoes an out-of-plane restricted internal rotation with symmetry number 2, barrier to rotation of 7 kcal mole$^{-1}$, and torsional oscillation frequency of about 425 cm$^{-1}$.[20] The model used for the transition state is included in Fig. 8. The O-H bond in nitric acid is extended by 0.18 Å to become a "half-order" bond,[21] and the new O-H bond being formed is also taken to be a half-order bond. The H-O-H angle is 105°, as in water, and the O-H bond in the approaching hydroxyl radical has the single-bond length of water. The hydrogen atom of the hydroxyl radical is "hydrogen bonded" to an oxygen atom in nitric acid to make a six-membered ring. The N-O bond distances

are taken to be the same as in nitric acid. The "reaction coordinate" is the oscillation of the hydrogen atom in the linear O-H-O, half-bonded segment. The potential energy gained by forming the new (1.73 Å) hydrogen bond presumably "pays for" the energy required for the other hydrogen atom to leave nitric acid and become part of the product water molecule.

According to transition-state theory,[15] the rate constant is

$$k = \kappa \left(\frac{kT}{h}\right) \frac{q'_{\ddagger}}{q_A q_B} \exp(-E/T) \qquad (11)$$

where $q_A$ and $q_B$ are molecular partition functions per unit volume respectively for $HNO_3$ and HO, $q'_{\ddagger}$ is the molecular partition function for the transition state omitting the reaction coordinate, $\kappa$ is the "transmission coefficient" or the probability per vibration of the O-H-O group that the water molecule will form and fly apart, and E is the activation energy in Kelvin units. In standard forms for translational and rotational partition functions, the rate constant may be expressed as

$$k = \kappa \left(\frac{kT}{h}\right)\left(\frac{M_{\ddagger}}{M_A}\right)^{3/2} \left[\frac{I_1 I_2 I_3\ {}^{\ddagger}}{I_1 I_2 I_3\ A}\right]^{1/2} \left(\frac{h^2}{2\pi M_B kT}\right)^{3/2} \left(\frac{h^2}{8\pi^2 I_B kT}\right) f\left(q_v\right) \qquad (12)$$

where the activation barrier is taken to be zero. The term $f(q_v)$ involves the vibrational partition functions for reactants and transition state

$$f\left(q_v\right) = \prod_{v}^{14} q_{\ddagger}/q_B \left(q_{ir} \prod_{v}^{8} q\right)_A \qquad (13)$$

where $q_{ir}$ refers to the restricted internal rotation in nitric acid and all other q's have the form

$$q = \left(1 - e^{-h\nu/kT}\right)^{-1} \qquad (14)$$

This model takes the electronic partition function of the transition state to be the same as that for the hydroxyl radical. At the low temperatures of this study, any vibrational frequency greater than about 1000 $cm^{-1}$ has a very small effect on the rate expression, and the key to a simple evaluation of (12) is to match up and cancel similar terms between the transition state and the reactants and to identify the low frequency terms that do not cancel.

The normal coordinates of nitric acid, hydroxyl radical, and the transition state are classified in Table 4 in terms of in-plane (||) and out-of-plane ($\perp$) motion, in terms of translational (tr) and rotational (rot) coordinates, and in terms of internal coordinates, including stretching (str), bending (b), internally rotating (i.r.), ring stretching and bending (ring), and reaction (rc) coordinates. In (12) the translations and rotations of $HNO_3$ and the transition state are expressed in ratio form, and the corresponding unmatched terms of HO appear in full. Nine vibrational modes are matched in Table 4; most of these have such high frequencies that their partition functions (14) are close to unity at these low temperatures; and even if the partition functions are slightly greater than one, these terms are effectively eliminated by matching and canceling. The unmatched normal coordinates in Table 4 are enclosed in parentheses. Aside from the translations and rotations of HO, these unmatched coordinates are the reaction coordinate, the internal rotation of nitric acid, and five vibrations (2 || and 3 $\perp$) of the six-membered ring of the transition state. The

ratio of vibrational partition functions (13) may be approximately reduced to the form

$$f(q) \sim \prod^{5} \left(q_v\right)_{\ddagger} / \left(q_{ir}\right)_A \quad . \tag{15}$$

One could assign force constants to the transition state and evaluate the vibration frequencies, but the assignment of force constants is no less arbitrary than assigning vibrational frequencies to the ring motions by analogy to other molecules. Pickett and Strauss[22] evaluated the ring bending frequencies of five molecules with single-bonded six-membered rings: cyclohexane, s-trioxane, p-dioxane, m-dioxane, and tetrahydropyran. The range of values was 229 to 752 $cm^{-1}$, and the average value was 421 $cm^{-1}$. The vibrational frequencies of gas-phase formic acid dimers were observed and analyzed.[23-25] These dimers involve a hydrogen-bonded eight-member ring, and identified ring-distortion frequencies were 243, 237, 232, 160, 103, and 60 $cm^{-1}$. The bonding in the transition state of Fig. 8 is "tighter" than the hydrogen-bonded dimer of formic acid and "looser" than the single-bonded rings in cyclohexane and related compounds. The transition state of Fig. 8 would be expected to have ring motions in the frequency range 100 to 1000 $cm^{-1}$, the higher end of the range made possible by the low mass of the hydrogen atoms.

The ratio of molecular weights contributes a factor of 1.43 to (12), the ratio of principal moments of inertia (Fig. 8) contributes a factor of 2.5 to (12), and the restricted rotor symmetry number is a factor of 2. With the physical and molecular constants and with these ratios, the theoretical rate-constant expression is

$$\frac{k}{cm^3\ s^{-1}} = \left(\frac{3.16 \times 10^{-10}}{T^{3/2}\ q_{ir}}\right)\left(q_{||}^{\ 2} q_{\perp}^{\ 3}\right)^{\ddagger} \qquad (16)$$

At low temperatures $q_{ir}$ has the form of (14) with a torsional frequency of 425 $cm^{-1}$. As a line of reference, the five frequencies of the transition state were set to very large values ($\infty$); and (16) was evaluated from 167 to 1000 K and plotted as the dashed curve in Fig. 9, which includes a heavy line based on the observed data. On this simple basis, the calculated rate is slower than that observed, whereas the problem seemed to be too low observed rate constant; and the reaction has a negative activation energy, but less in magnitude than that observed. The five frequencies of the transition state were set equal, assigned values between 1000 and 200 $cm^{-1}$, and the rate expression (16) was evaluated between 1000 and 167 K, Fig. 9. As the assigned frequencies are decreased, the absolute value of the rate constant increases to give better agreement with observed values, but the temperature dependence moves further away from that observed. At low frequencies, around 200 $cm^{-1}$, the rate constant increases with increasing temperature. One might expect the hydrogen-atom motions to have higher frequencies than the motions of oxygen and nitrogen atoms. On this basis, two frequencies were set to 1000 $cm^{-1}$ and the other three varied between 800 and 150 $cm^{-1}$. The fan of calculated curves is similar to that in Fig. 9, and no set of frequencies could be found that more-or-less matched both the absolute values and the slope (vs T) of the observed rate constants.

Perhaps this discussion should be dropped here, with the assessment that simple transition state theory semi-quantitatively accounts for the low pre-exponential factor and some negative activation energy. The discrepancies would then be ascribed to the simplicity of the theory and the crude method of handling the structural model. However, further considerations of the simple theory suggest an additional interpretation.

What is needed to fit the model to the data is a higher power of T in the denominator of (12) and (16). The observed power of temperature in the rate expression is -2.29, Fig. 6. The power of temperature in the theoretical expression (16) is -1.5, and any departure of $q_v$ from the low-temperature limit of unity would tend to increase this value. There is no way for (16) to give a value less than -1.5. However, (16) may be rewritten as

$$\underline{k} = \frac{(\kappa\, kT/h)\ 1.52 \times 10^{-20}}{T^{5/2} q_{ir}} \left(q_{||}^{2} q_{\perp}^{3}\right)_{\ddagger} \qquad (17)$$

and one may re-examine the term ($\kappa$ kT/h) in the numerator of (17).

In the simplest derivation of transition-state theory, the transition state is said to move toward products with a frequency $\nu^*$ and this co-ordinate is ascribed a partition function of the form of (14). The reaction coordinate is assumed to have a low frequency such that (14) reduces to the classical-mechanical limit, $kT/h\nu^*$

$$\nu^* q^* = \nu^* \left(1 - e^{-h\nu^*/kT}\right)^{-1} \longrightarrow kT/h \qquad (18)$$

and the unknown frequency of the reaction coordinate cancels to give the universal frequency kT/h. In the present case the reaction co-ordinate in the vibration of a hydrogen atom between two oxygen atoms

in a six membered ring. The reaction coordinate is primarily a hydrogen atom motion, and the frequency could be 1000 $cm^{-1}$ or higher. For comparison the hydrogen stretching motions in a hydrogen bond have frequencies in the range 2500-3500 $cm^{-1}$,[26] but this motion is not strictly comparable to the symmetrically placed hydrogen atom in Fig. 8. Even at 1000 $cm^{-1}$ the reaction coordinate should be treated by quantum mechanics, not in the sense of quantum mechanical tunneling since there is no activation barrier, but in consideration of the size of one cell in phase space. If $\nu^*$ is larger than kT/h, the partition function $q^*$ has the temperature independent value of about one. In this case $\kappa\nu^* q^*$ becomes $\kappa\nu^*$, not $\kappa kT/h$, and with $\nu^*$ in units of $cm^{-1}$ the rate expression is

$$\underline{k} = \frac{(\kappa\nu^*)\ 4.56 \times 10^{-10}}{T^{5/2} q_{ir}} \left(q_{||}^{\ 2} q_{\perp}^{\ 3}\right)_{\ddagger} \qquad (19)$$

Another derivation of transition-state theory involves a distance $\delta$, across which one calculates the reaction frequency $p/m\delta$; and the classical partition function is $\delta/\Lambda$ where $\Lambda$ is the Boltzmann-average de Broglie wavelength $h/(2\pi mkT)^{1/2}$. This component of rate is integrated over the classical-mechanical Boltzmann distribution of momentum and over the reaction coordinate for the distance $\delta$ to produce the expression kT/h. Since in this problem there is no potential energy barrier, one may assign $\delta$ an unusually large value, say 0.1 Å, compare Fig. 8. In this case at room temperature, the Uncertainty-Principle momentum for a hydrogen atom corresponds to a zero-point energy along the reaction coordinate that exceeds kT by a factor of 8, whereas it should be much

less than kT to justify the continuous integrations that are carried out. Even along the constant potential-energy channel, the reaction coordinate involves an almost temperature-independent quantum-mechanical frequency factor related to zero-point energy.

The rate constant $\underline{k}$ was evaluated from (19) using several sets of transition-state frequencies as adjustable parameters. For values of $\nu_{||}$ and $\nu_{\perp}$ used in Fig. 9 and in other similar calculations, the value of $(\kappa\nu^*)$ was adjusted to give $\underline{k} = 9.0 \times 10^{-14}$ cm$^3$ s$^{-1}$ at 400 K, and then the effect of temperature from 400 to 200 K was predicted. This procedure is illustrated for eight sets of frequencies in Table 5 and in Fig. 10. The upper panel in Fig. 10 includes the observed points by Wine et al.[1] and this study, the lower panel gives only the observations in this study. All eight of these sets of frequencies give satisfactory agreement between theory and experiment. The values of $(\kappa\nu^*)$ range between 244 and 551 cm$^{-1}$. The best agreement with experiment comes from values of the ring frequencies: 1000 (twice) and about 450 (three times), or alternatively by about 550 cm$^{-1}$ (five times). These frequencies are within the range of those observed in single-bonded six membered rings[22] and are somewhat higher than those observed in a hydrogen-bonded eight-member ring.[23-25] Although the value of $\kappa$ is indeterminate in this analysis, the value of $\kappa\nu^*$ is within the expected range, especially if $\kappa$ is 0.5 or somewhat less. The ring-deformation frequencies fitted here to the activated complex are somewhat higher than expected.

It is well to recall alternative physical explanations to the language of transition state theory. The partition functions do not represent time averages over one collision, but rather are ensemble averages.[15] The meaning of the tightly bound six-membered ring is that the molecule $HNO_3$ and the radical HO must collide in a constrained solid angle so that the potential energy gained by the transient intermolecular hydrogen bond compensates for a potential energy barrier in other parts of the collision complex. The limited volume of phase space for these constrained angles of approach are expressed in other words as a ring structure.

It is not claimed that this model and these vibration frequencies represent the transition-state-theory solution to the rate of this reaction. Rather this theoretical study indicates that it may not be necessary to postulate a complex mechanism for this reaction. The simple transition-state method, modified to have a quantum-mechanical reaction coordinate, is capable of explaining the magnitude and the temperature dependence of this rate in terms of a tight cyclic transition state, whose frequencies are marginally within the range of those expected.

## The Reaction of HO with $H_2O_2$

At 298 K the rate constant for (2) is twelve times that for (1), and the ratio of pre-exponential factors, $A_2/A_1$, is 165. If the discussion above gives a semi-quantitative account of the low value of $k_1$ and of its increase with decreasing temperature, one should use the same language to compare reaction (2) to reaction (1). The model of the transition state of reaction (2) is taken to be a zig-zag six-membered

chain, with a linear O···H···O segment. Such a structure would have two internal-rotation coordinates. In comparing $k_2$ and $k_1$, all reference to the hydroxyl radical cancels out, the ratio of molecular weights and moments of inertia (compare Eq. 12) are not greatly different for the two cases, and similar frequencies can be cancelled between transition state and reactant ($HNO_3$ or $H_2O_2$). To a reasonable approximation, the ratio of rate constants is

$$\frac{k_2}{k_1} = \frac{\left(q_{ir}\right)_A}{\left(q_{ir}\right)_P} \frac{\left(q_{ir}^{\,2} q_v^{\,3}\right)_{\ddagger P}}{\left(q_v^{\,5}\right)_{\ddagger A}} \approx \frac{\left(q_{ir}\right)^2_{\ddagger P}}{\left(q_v\right)^2_{\ddagger A}} \qquad (20)$$

where A refers to nitric acid and P refers to peroxide. The vibration frequencies of the ring structure in the transition state for (1) were assigned values of about 400 cm, for which the value of the partition function is about 1.2 at 298 K. If the reduced moment of inertia for the internal rotation of the transition state in (2) is taken to be $1 \times 10^{-40}$ g cm$^2$ (the value of the lowest principal moment of inertia in $H_2O$), the partition function for free internal rotation is about 5 at 298 K. The square of 5/1.2 is 17, and thus (20) indicates that $k_2$ could easily exceed $k_1$ by the observed factor of 12 at 298 K.

The "free internal rotations of the transition state" of reaction (2) can also be expressed in other words. As the oxygen atom of the hydroxyl radical approaches a hydrogen atom on $H_2O_2$, a large solid-angle of approach leads to reaction, and for each satisfactory line of this approach the orientation of the hydrogen atom on the hydroxyl radical can take on $2\pi$ values about the third Euler angle $\chi_r$. This situation is to be contrasted with reaction (1) where both O and H in HO must

hit an H and O in $HNO_3$ in a constrained manner. Transition-state theory provides a simple method to demonstrate that this difference is large enought to account for the differences observed in the rates of reactions (1) and (2).

Acknowledgment

This work was supported by the Director, Office of Energy Research, Office of Basic Energy Sciences, Chemical Sciences Division of the U.S. Department of Energy under Contract No. DE-AC03-76SF00098.

References

1. P. H. Wine, A. R. Ravishankara, N. M. Kreutter, R. C. Shah, J. M. Nicovich, R. L. Thompson and D. J. Wuebbles, J. Geophys. Res. 86, 1105 (1981).

2. M. J. Kurylo, K. D. Cornett and J. L. Murphy, J. Geophys. Res. accepted for publication 1982.

3. R. Zellner and I. W. M. Smith, Chem. Phys. Lett. 26, 72 (1974).

4. I. W. M. Smith and R. Zellner, Int. J. Chem. Kinet. Symposium 1, 341 (1975).

5. J. J. Margitan, F. Kaufman and J. G. Anderson, Int. J. Chem. Kinet. Symposium 1, 281 (1975).

6. H. H. Nelson, W. J. Marinelli and H. S. Johnston, Chem. Phys. Lett. 78, 495 (1981).

7. D. Husain and R. G. W. Norrish, Proc. Royal Soc. A. 273, 165 (1963).

8. L. F. Keyser, J. Phys. Chem. 84, 1659 (1980).

9. U. C. Sridhara, B. Reimann and F. Kaufman, J. Chem. Phys. 73, 1286 (1980).

10. H. H. Nelson, Ph.D. Thesis, University of California, Berkeley, and Lawrence Berkeley Laboratory Report LBL-11666, 1980.

11. P. H. Wine, D. H. Semmes and A. R. Ravishankara, J. Chem. Phys. 75, 4390 (1981).

12. N. R. Greiner, J. Phys. Chem. 72, 406 (1968).

13. W. Hack, K. Hoyermann and H. G. Wagner, Int. J. Chem. Kinet. Symposium 1, 329 (1975).

14. G. W. Harris and J. N. Pitts, J. Chem. Phys. 70, 2581 (1979).

15. H. S. Johnston, Gas Phase Reaction Rate Theory, The Ronald Press Co., New York, 1966.

16. F. Magnotta, Ph.D. Thesis, University of California, Berkeley, and Lawrence Berkeley Laboratory Report LBL-9981, 1979.

17. P. H. Wine, N. M. Kreutter and A. R. Ravishankara, J. Phys. Chem. 83, 3191 (1979).

18. L. T. Molina and M. J. Molina, J. Photochem. 15, 97 (1981).

19. C. Morley and I. W. M. Smith, J. Chem. Soc. Faraday Trans. II 68, 1016 (1972).

20. W. R. Forsythe and W. F. Giauque, J. Am. Chem. Soc. 64, 529 (1942).

21. L. Pauling, The Nature of the Chemical Bond (Third Edition), Cornell University Press, 1960, p. 255.

22. H. M. Pickett and H. L. Strasuss, J. Chem. Phys. 53, 376 (1970).

23. R. C. Milliken, Ph.D. Thesis, University of California, Berkeley, 1957.

24. T. Miyazawa and K. S. Pitzer, J. Am. Chem. Soc. 81, 74 (1959).

25. L. Bonner and J. S. K. Smith, Phys. Rev. 57, 1078 (1940).

26. G. C. Pimentel and A. L. McClellan, The Hydrogen Bond, W. H. Freeman and Co., San Francisco, 1960, p. 68.

Table 1. Summary of flash-photolysis/resonance-fluorescence results for the reaction of HO with $HNO_3$.

| Pressure Torr | Flow rate in cell[a] cm $s^{-1}$ | $\frac{T}{K}$ | No. of runs | $\frac{k_1 \pm 2\sigma}{10^{-14}}$ $cm^3$ $s^{-1}$ | $k_1$ ave[b] |
|---|---|---|---|---|---|
| 10 | 18 | 363 | 9 | 10.4 ± 1.6 | 9.6 ± 2.4 |
| 25 | 18 | | 5 | 9.2 ± 1.2 | |
| 10 | 18 | 323 | 5 | 11.2 ± 2.0 | 10.6 ± 2.6 |
| 25 | 18 | | 6 | 10.4 ± 1.3 | |
| 10 | 25[c] | 298 | 21 | 13.5 ± 1.7 | 13.1 ± 2.4 |
| 10 | 25[c,d] | | 6 | 14.0 ± 2.7 | |
| 10 | 25[c] | | 4 | 13.6 ± 2.0 | |
| 10 | 12[c] | | 4 | 13.6 ± 3.6 | |
| 10 | 18 | | 6 | 12.8 ± 1.7 | |
| 25 | 25[c] | | 8 | 13.5 ± 1.7 | |
| 25 | 18 | | 6 | 12.1 ± 1.5 | |
| 50 | 25[c] | | 6 | 13.3 ± 1.7 | |
| 10 | 18 | 273 | 5 | 14.8 ± 2.2 | 15.2 ± 2.6 |
| 25 | 18 | | 5 | 15.4 ± 1.8 | |
| 10 | 18 | 250 | 5 | 19.3 ± 2.9 | 19.6 ± 3.2 |
| 25 | 18 | | 5 | 19.9 ± 2.8 | |
| 10 | 18 | 218 | 7 | 30.8 ± 4.2 | 30.4 ± 4.6 |
| 25 | 18 | | 5 | 30.0 ± 3.6 | |

[a]Flow rate through interaction region; [b]Error limits cover ± 2σ of all points; [c]Performed in first cell; other points in cell of Fig. 2; [d]UV absorption cell placed after photolyis cell; place before cell on other runs.

Table 2. Summary of kinetic results for the reaction of HO with $HNO_3$

| Temp. K | $\frac{k_{298}}{10^{-13}}$ [a] | $\frac{A}{10^{-14}}$ [a] | E/R [b] K | Method [c] | Ref. |
|---|---|---|---|---|---|
| 298 | 1.7 | - | - | FP/KS | 7 |
| 208 | 1.3 | - | - | FP/RA | 19 |
| 230-490 | 0.90 | 9.0 | 0 | FP/RA | 3 |
| 228-472 | 0.80 | 8.0 | 0 | FP/RA | 4 |
| 270-470 | 0.89 | 8.9 | 0 | DF/RF | 5 |
| 298 | 0.82 | - | - | FP/RF | 6 |
| 224-366 | 1.34 | 1.52 | -649 | FP/RF | 1 |
| 225-300 [d] | 1.34 | 1.05 | -759 | FP/RF | 2 |
| 218-363 | 1.32 | 1.52 | -644 | FP/RF | this work |

[a] $cm^3$ $molecule^{-1}$ $s^{-1}$.

[b] $k = A \exp(-E/RT)$.

[c] FP, flash photolysis; KS, kinetic absorption spectroscopy; RA, resonance absorption; DF discharge flow; RF, resonance fluorescence.

[d] The observed points deviated from the Arrhenius function above 300 K.

Table 3. Summary of kinetic results for the reaction of HO with $H_2O_2$

| Temp. K | $\frac{k_{298}}{10^{-12}}$ [a] | $\frac{A}{10^{-12}}$ [a,b] | E/R [b] K | Method [c] | Ref. |
|---|---|---|---|---|---|
| 300-458 | 0.93 | 0.41 $T^{1/2}$ | 604 | FP/KS | 12 |
| 298-670 | 0.84 | 7.97 | 670 | DF/ESR | 13 |
| 298 | 0.68 | - | - | FP/RF | 14 |
| 225-423 | 1.64 | 2.51 | -126 | DF/RF | 8 |
| 250-459 | 1.69 | 2.96 | -163 | DF/LIF | 9 |
| 298 | 1.57 | - | - | FP/RF | 10 |
| 273-410 | 1.57 | 3.7 | -260 | FP/RF | 11 |
| 298 | 1.81 | - | - | FP/RF | this work |

[a] $cm^3$ $molecule^{-1}$ $s^{-1}$.

[b] $k = A \exp(-E/RT)$.

[c] See Table 2. Also: ESR, electron spin resonance; LIF, laser induced fluorescence.

Table 4. Classification and matching of normal coordinates in the reactants and in the transition state for the reaction HO + $HNO_3$

| In-plane (\|\|) motions | | | Out-of-plane ($\perp$) motions | | |
|---|---|---|---|---|---|
| ‡ | $HNO_3$ | HO | ‡ | $HNO_3$ | HO |
| 2 tr | 2 tr | | 1 tr | 1 tr | |
| 1 rot | 1 rot | | 2 rot | 2 rot | |
| | | (2 tr) | | | (1 tr) |
| | | (1 rot) | | | (1 rot) |
| 3 $NO_3$ str | 3 $NO_3$ str | | 1 $NO_3$ b | 1 $NO_3$ b | |
| 2 $NO_3$ b | 2 $NO_3$ b | | | | |
| 2 $H_2O$ str | 1 HO str | 1 HO str | | | |
| 1 $H_2O$ b | 1 HON b | | | | |
| | | | | (1 i.r.) | |
| (2 ring) | | | (3 ring) | | |
| (1 r.c.) | | | | | |
| TOTAL: 14 | 10 | 4 | 7 | 5 | 2 |

Table 5. Parameters adjusted to obtain the calculated curves in Fig. 10, k (400 K) adjusted to give $\kappa\nu^*$

| $\nu(\|\|)$ / $cm^{-1}$ | $\nu(\perp)$ / $cm^{-1}$ | $\kappa\nu^*$ / $cm^{-1}$ |
|---|---|---|
| 1000 | 600 | 482 |
| 1000 | 500 | 404 |
| 1000 | 400 | 310 |
| 1000 | 350 | 256 |
| 800 | 800 | 551 |
| 600 | 600 | 399 |
| 500 | 500 | 299 |
| 450 | 450 | 244 |

Figure Captions

Figure 1. Schematic diagram of FP/RF apparatus. Resonance lamp is shown on PMT axis but actually is perpendicular.

Figure 2. Schematic diagram of reaction cell, resonance lamp and detector geometries. PMT, RCA 31034 photomultiplier tube; BRP, 309 nm interference filter; B1 and B2, scattered light baffles; F, Hoya "Peak 320" color filter; W1, $CaF_2$ window; L1, 1-1/2" dia. x 2" f.l. Suprasil-1 lense; L2, 1" dia. x 1-12/" f.l. Suprasil-1 lense; W2, Vycor resonance lamp window; RL, resonance lamp; MC, microwave cavity: WH, Woods horn; LA, photolysis laser axis; RC, reaction cell interaction region; RCOJ, reaction cell temperature control outer jacket; VH, vacuum housing; RMI, reaction mixture in; RMO, reaction mixture pump out.

Figure 3. An example of HO decay in nitric acid (compare Eq. 4). Dots, experimental data; solid line, least squares fit, which starts 1 ms after laser fires. The slope gives pseudo-first-order rate constant (7).

Figure 4. Plot of pseudo-first-order rate constants against $[HNO_3]$ for the reaction of HO with $HNO_3$. The slopes give the second order rate constants, $k_1$ = (1.35, 1.35, 1.33) x $10^{-13}$ $cm^3$ $molecule^{-1}$ $s^{-1}$, at 10, 25, and 50 Torr respectively.

Figure 5. Arrhenius plot for the reaction of HO with $HNO_3$ from 218-363 K.

Figure 6. Test of the temperature expression $k = BT^n$ for the reaction of HO with $HNO_3$ from 218-363 K.

Figure 7. First order plot for the reaction of HO with $H_2O_2$ at 298 K and 10 Torr.

Figure 8. Structure of nitric acid molecule and the $HO \cdot HNO_3$ transition state considered in this study.

Figure 9. Comparison of observed and calculated rate constants for reaction (1) for a range of assigned ring-motion frequencies of the transition state of Fig. 8. The calculated curves are based on Eq. 16, and all five frequencies are assigned the frequencies ($cm^{-1}$) indicated by the numbers on this figure. For high frequencies the rate is lower than that observed, and there is a modest negative activation energy. As the assigned frequencies are raised, there is agreement between observed and calculated rate constants at one temperature at a time, but the observed temperature dependence is not matched.

Figure 10. Calculated curves and observed rate constants: triangles, Ref. 1; circles, this work. The curves are calculated by means of (19). The five "new" frequencies of the transition state are the numbers given ($cm^{-1}$) taken five times for the lower panel; three equal frequencies are assigned the numbers given in the upper panel and the other two are assigned 1000 $cm^{-1}$. In each case ($\kappa\nu^*$) of (19) is adjusted to give agreement between theory and experiment at 400 K; these values are listed in Table 5.

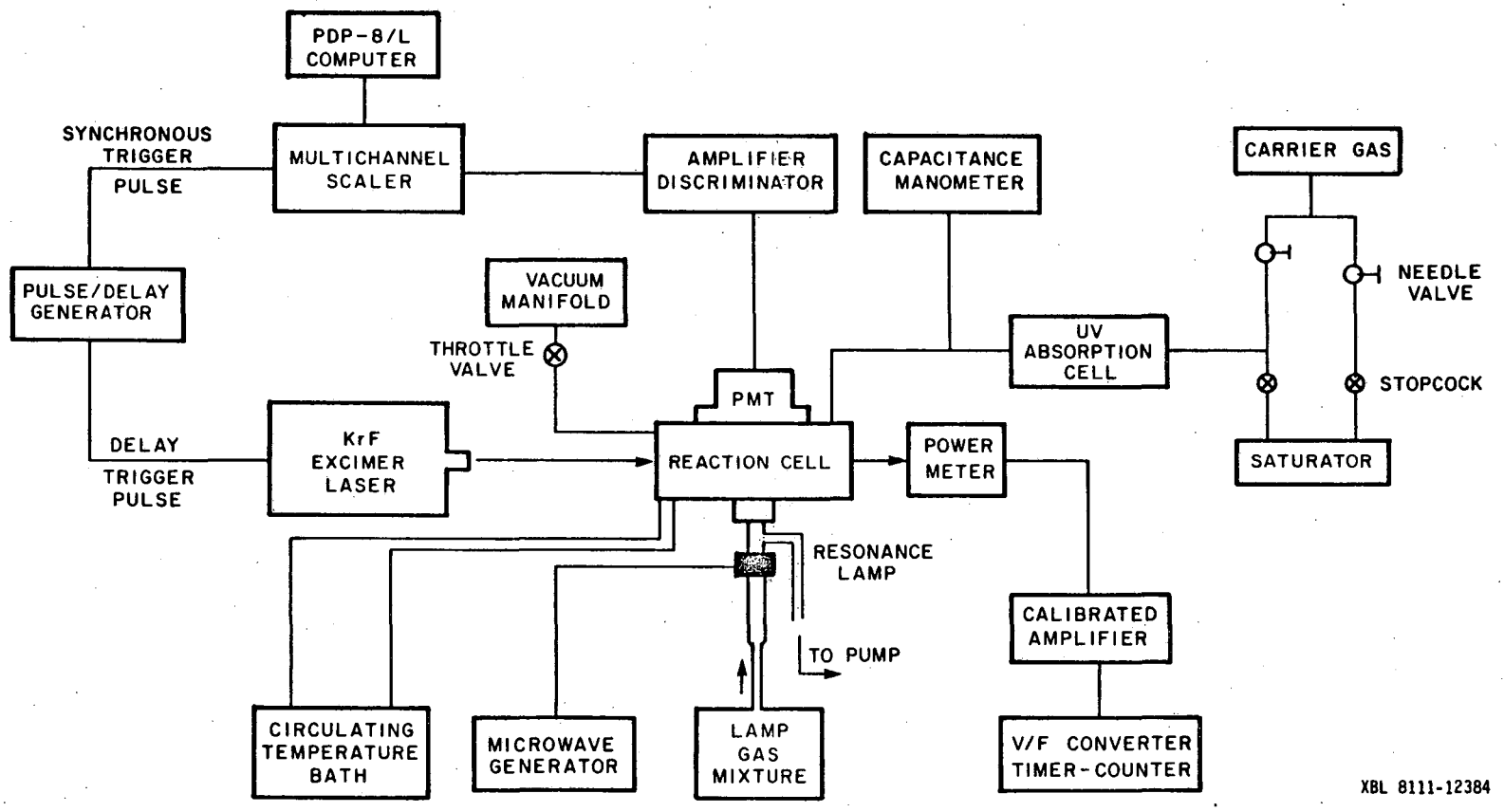
PDP-8/L COMPUTER
SYNCHRONOUS TRIGGER PULSE
MULTICHANNEL SCALER
AMPLIFIER DISCRIMINATOR
CAPACITANCE MANOMETER
CARRIER GAS
PULSE/DELAY GENERATOR
VACUUM MANIFOLD
THROTTLE VALVE
NEEDLE VALVE
UV ABSORPTION CELL
PMT
STOPCOCK
DELAY TRIGGER PULSE
KrF EXCIMER LASER
REACTION CELL
POWER METER
SATURATOR
RESONANCE LAMP
CALIBRATED AMPLIFIER
TO PUMP
CIRCULATING TEMPERATURE BATH
MICROWAVE GENERATOR
LAMP GAS MIXTURE
V/F CONVERTER TIMER-COUNTER
XBL 8111-12384

Fig. 1

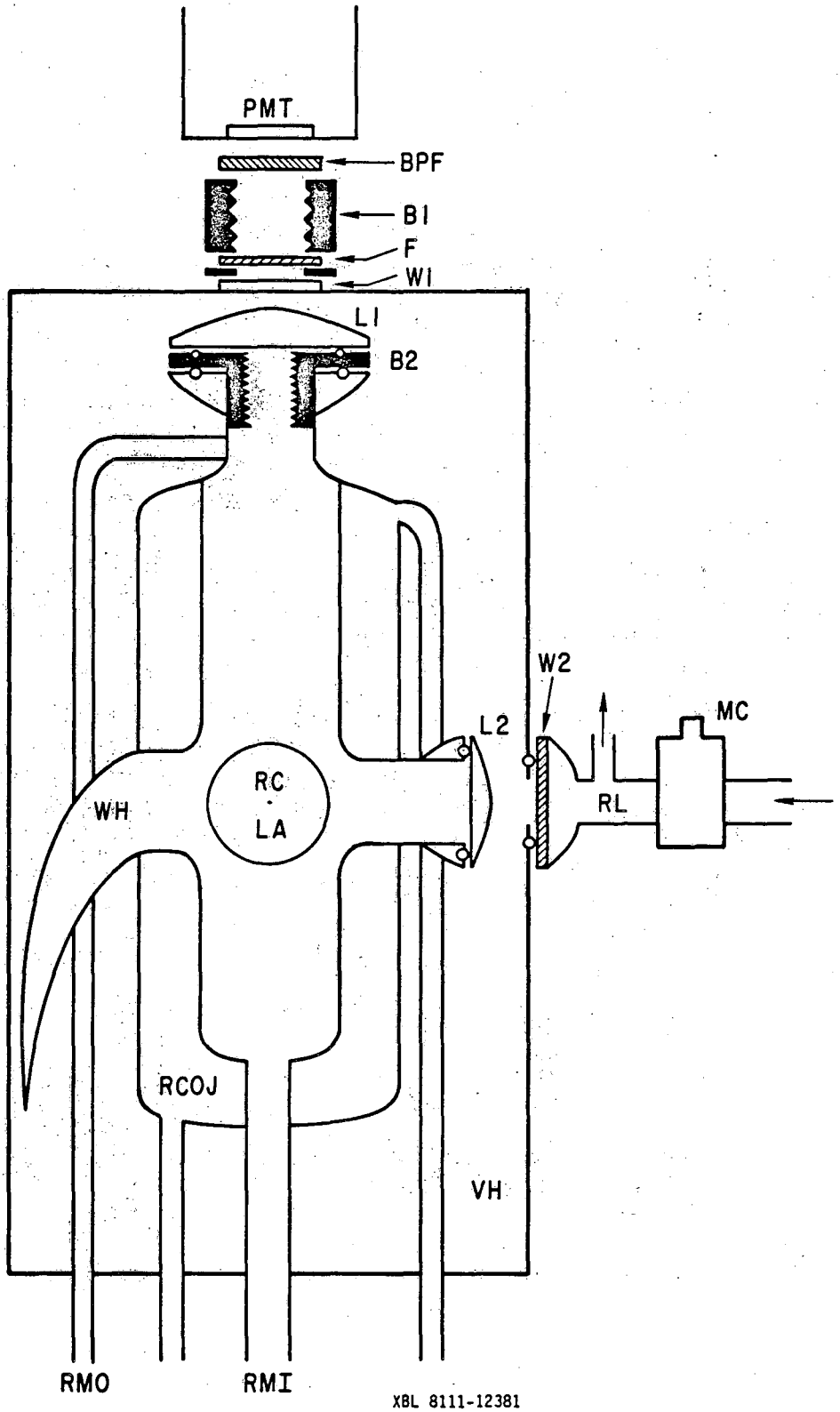
PMT
BPF
B1
F
W1
L1
B2
W2
MC
L2
RC
LA
WH
RL
RCOJ
VH
RMO
RMI
XBL 8111-12381

Fig. 2

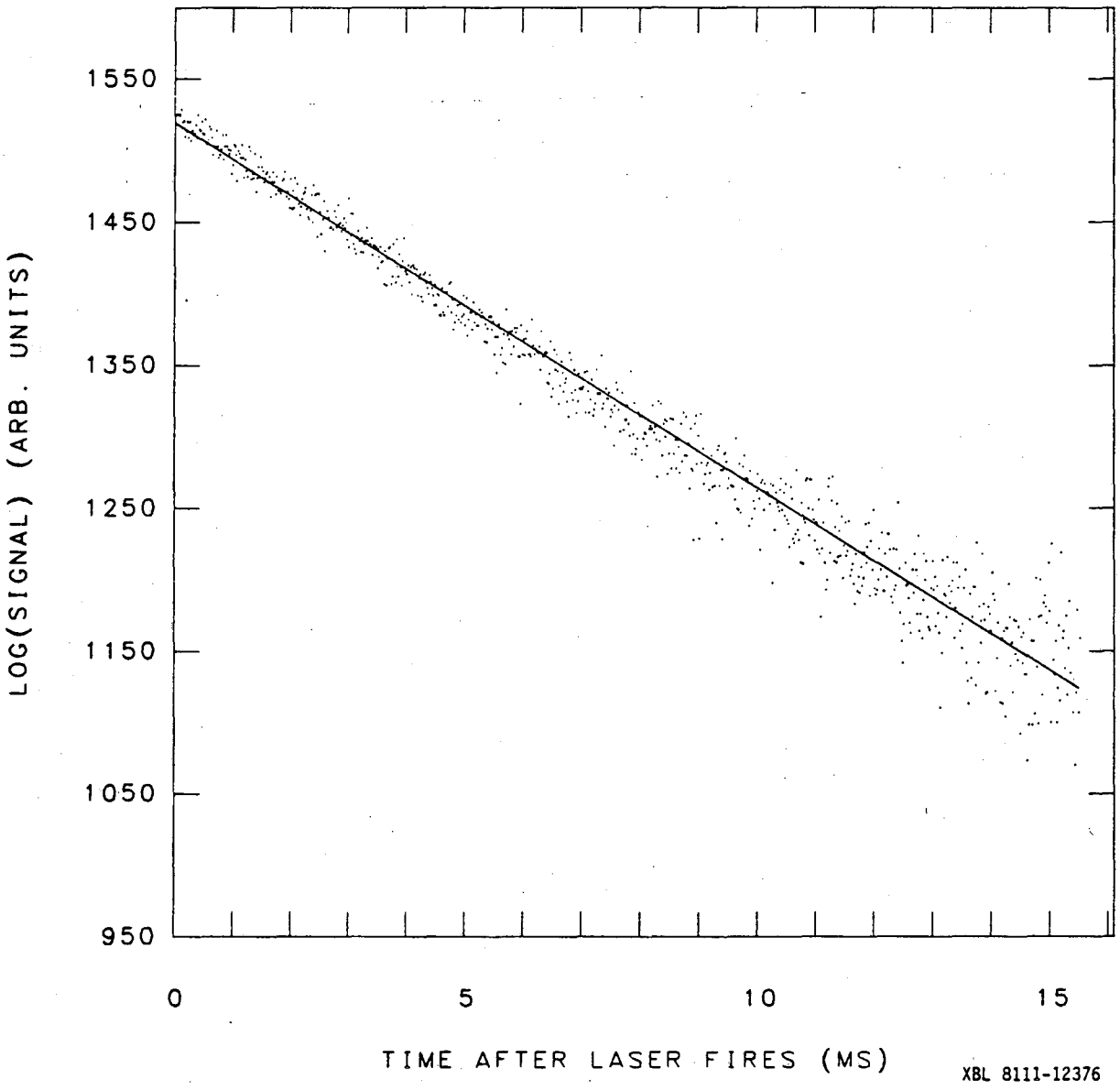
1550
1450
1350
1250
1150
1050
950
LOG(SIGNAL) (ARB. UNITS)
0
5
10
15
TIME AFTER LASER FIRES (MS)
XBL 8111-12376

Fig. 3

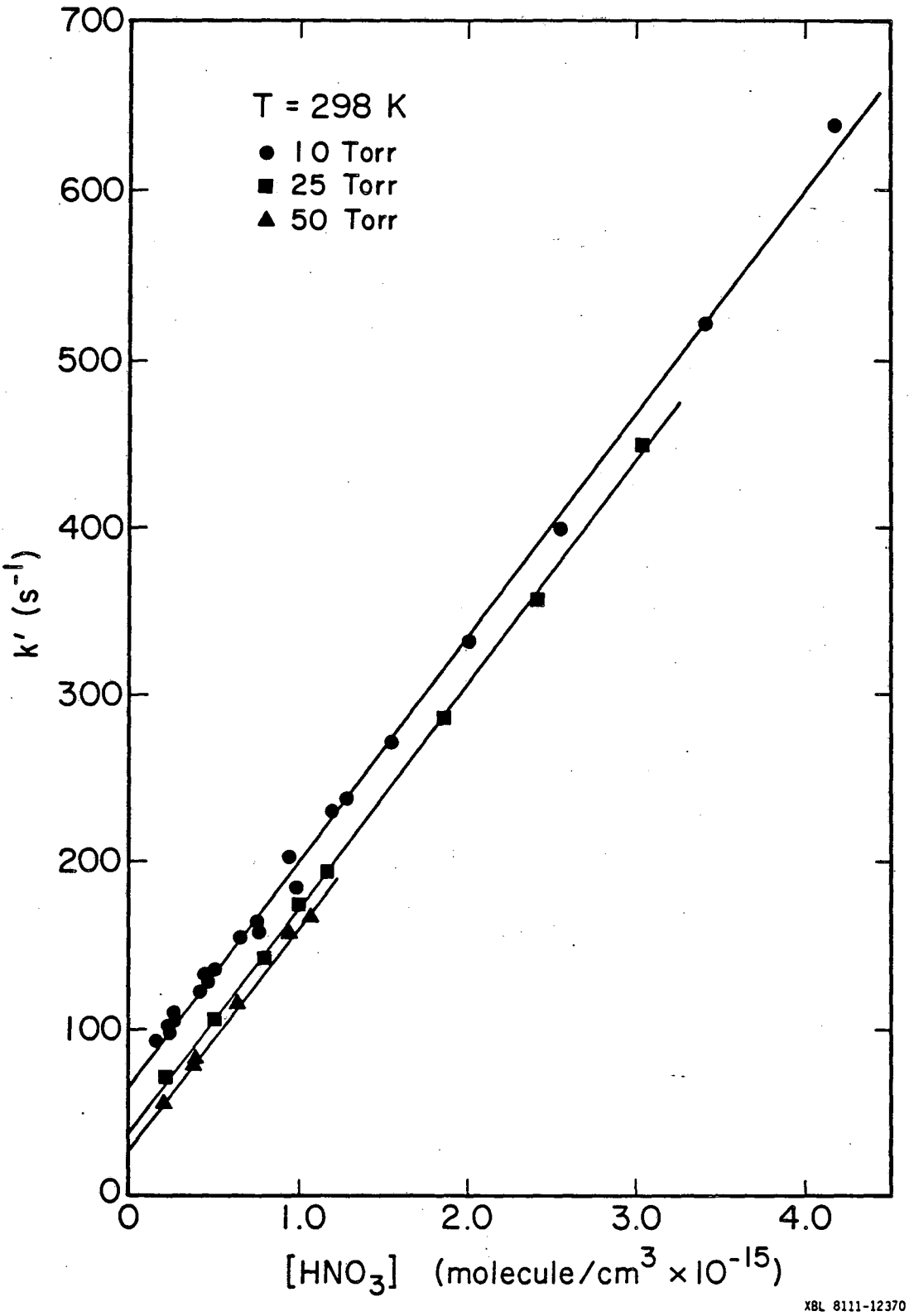
T = 298 K
● 10 Torr
■ 25 Torr
▲ 50 Torr
k' (s⁻¹)
[HNO3] (molecule/cm³ × 10⁻¹⁵)
0
100
200
300
400
500
600
700
1.0
2.0
3.0
4.0
XBL 8111-12370

Fig. 4

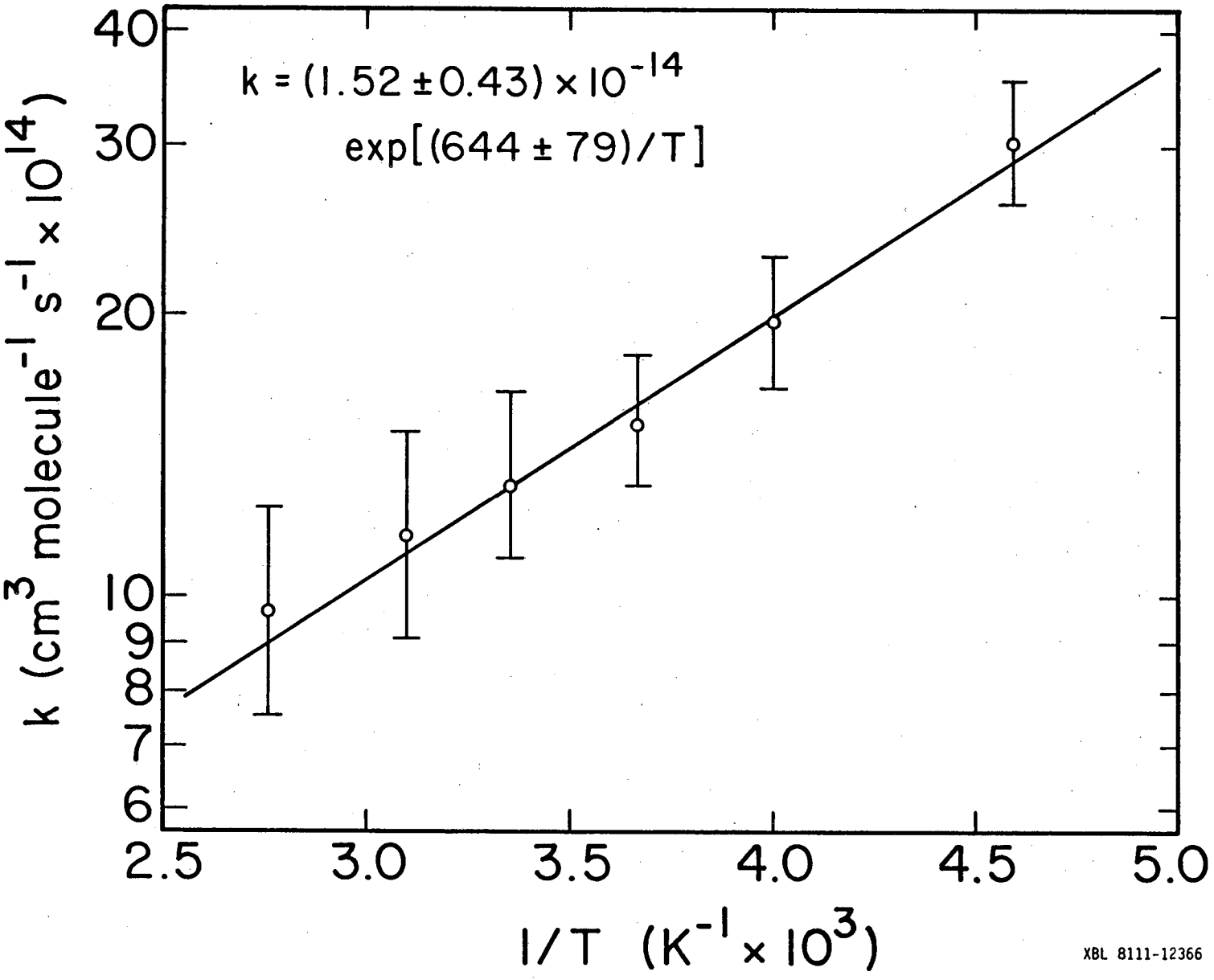
k = (1.52 ± 0.43) × 10^-14
exp[(644 ± 79)/T]
k (cm^3 molecule^-1 s^-1 × 10^14)
40
30
20
10
9
8
7
6
2.5
3.0
3.5
4.0
4.5
5.0
1/T (K^-1 × 10^3)
XBL 8111-12366

Fig. 5

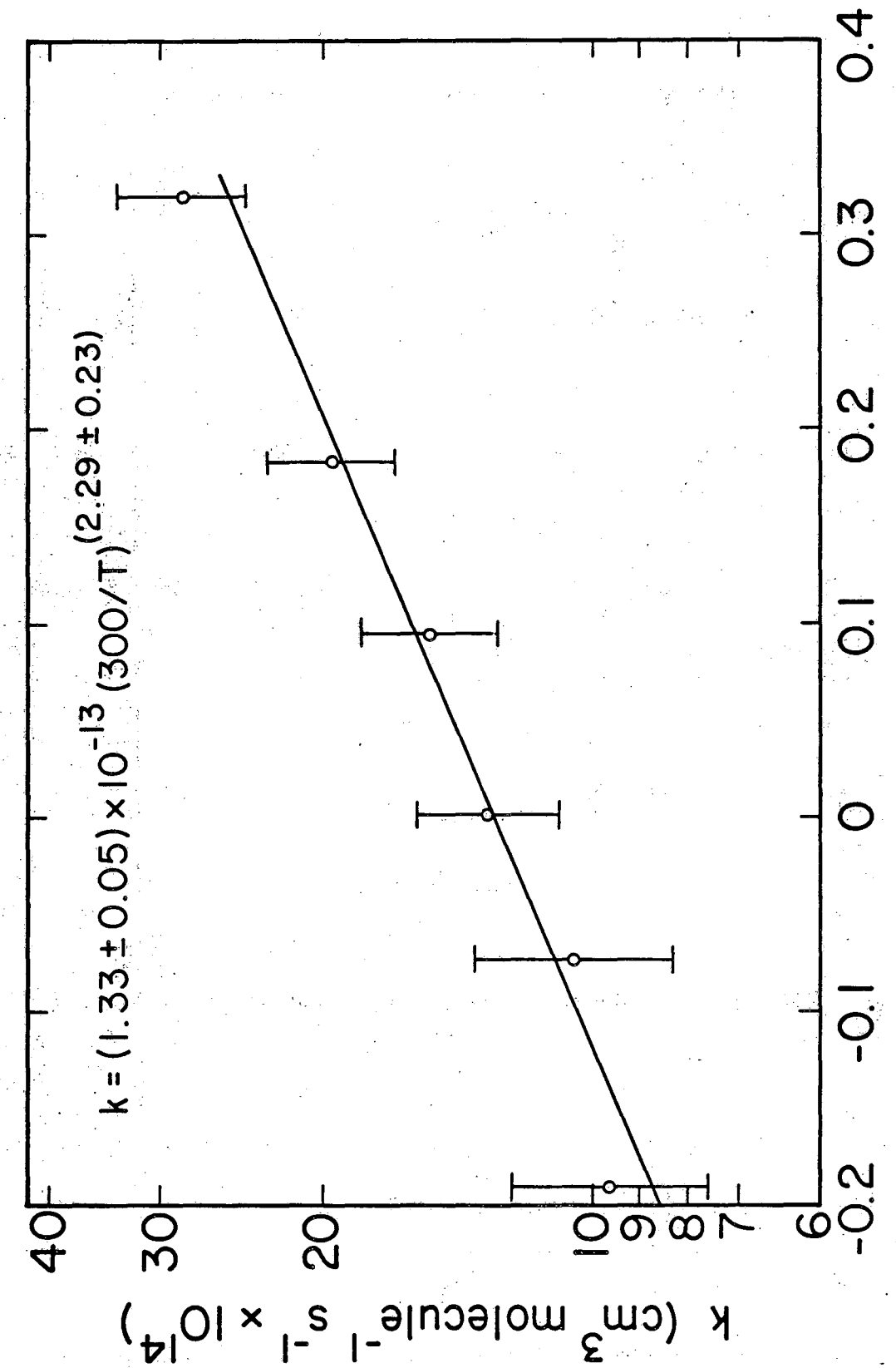


XBL 8111-12367

Fig. 6

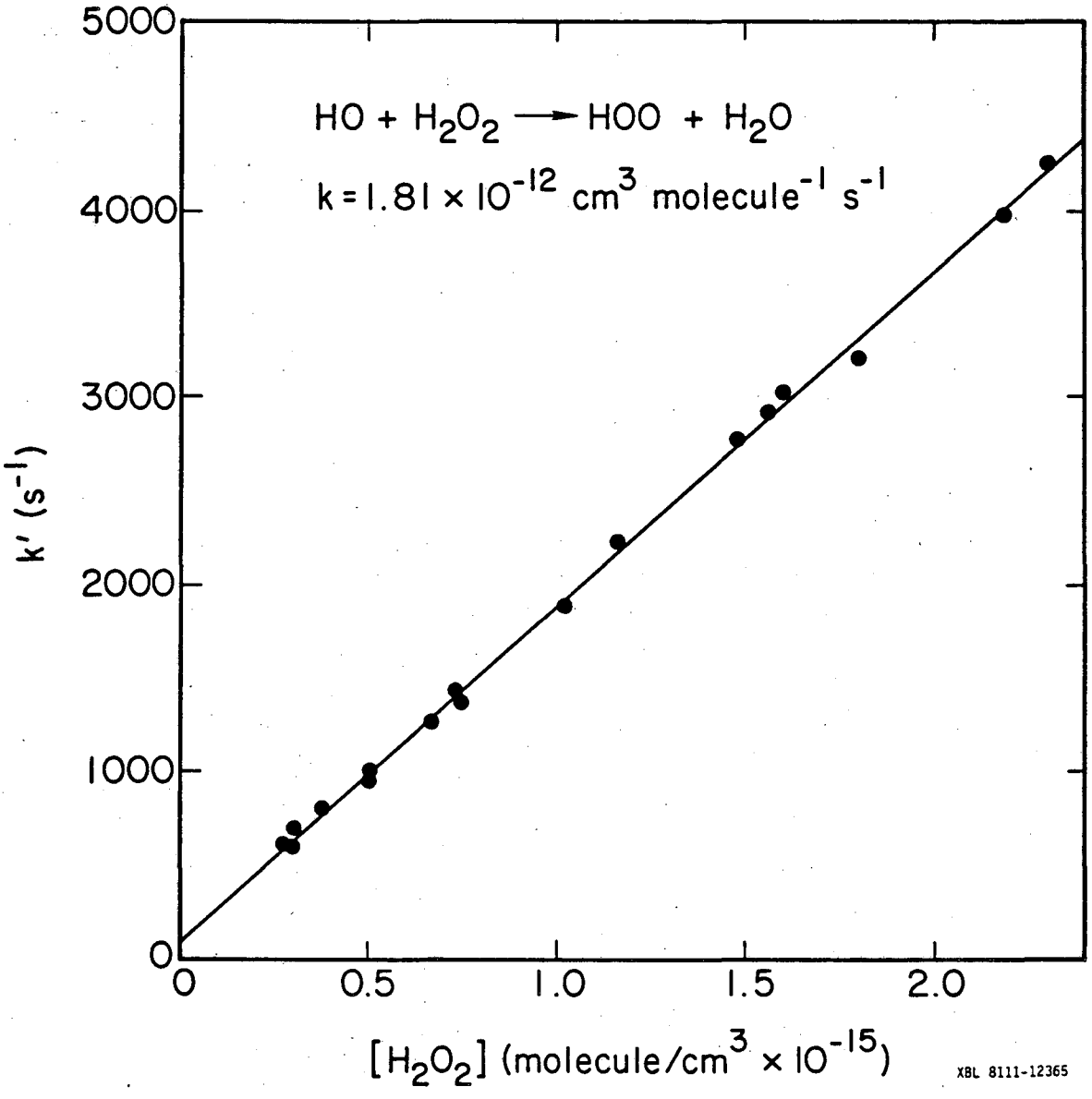
HO + H2O2 → HOO + H2O
k = 1.81 × 10-12 cm3 molecule-1 s-1
5000
4000
3000
2000
1000
0
k' (s-1)
0
0.5
1.0
1.5
2.0
[H2O2] (molecule/cm3 × 10-15)
XBL 8111-12365

Fig. 7

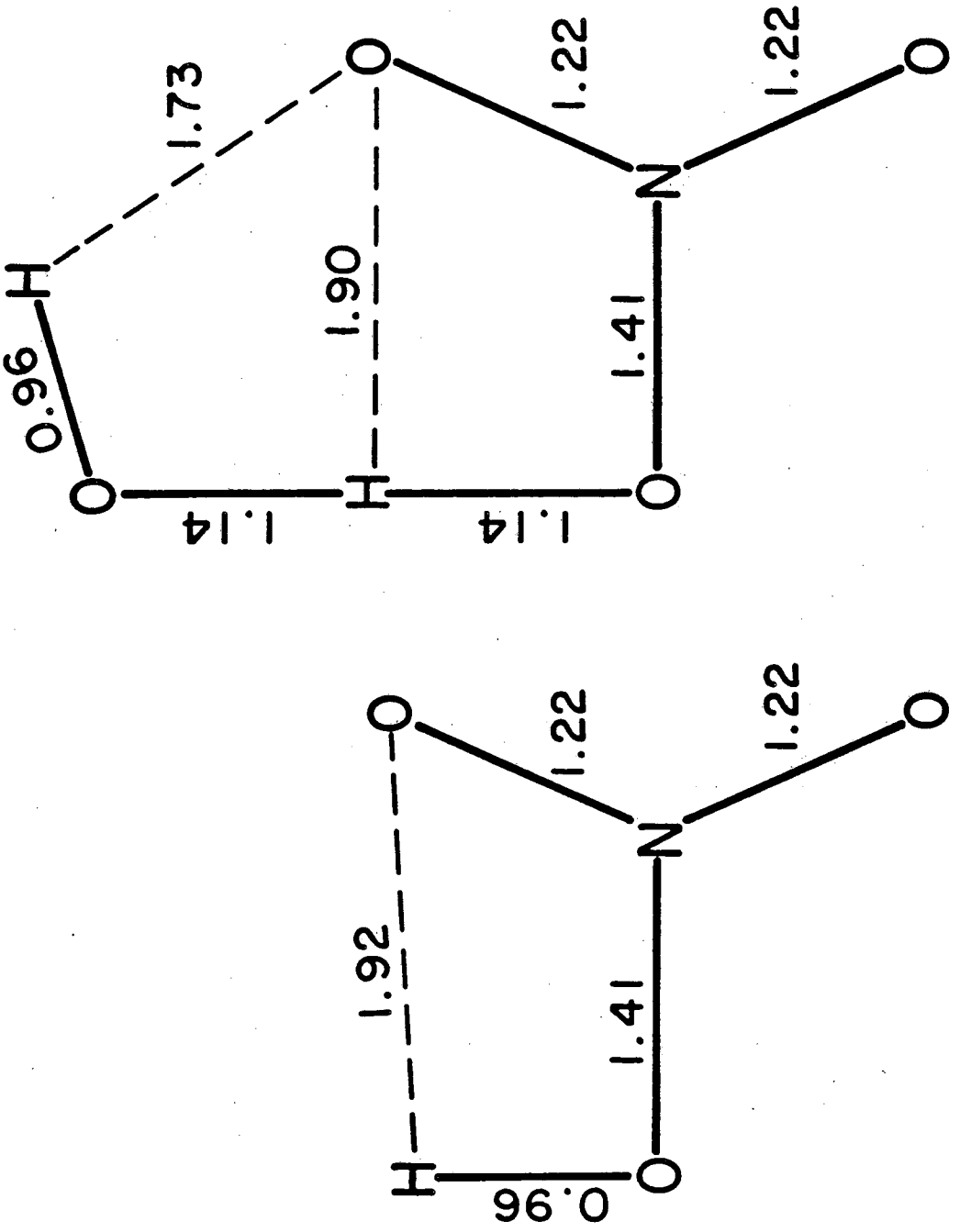
1.73
O
1.22
1.22
O
H
1.90
N
1.41
0.96
O
H
O
1.14
1.14
1.22
1.22
O
N
1.92
1.41
H
O
0.96

Fig. 8

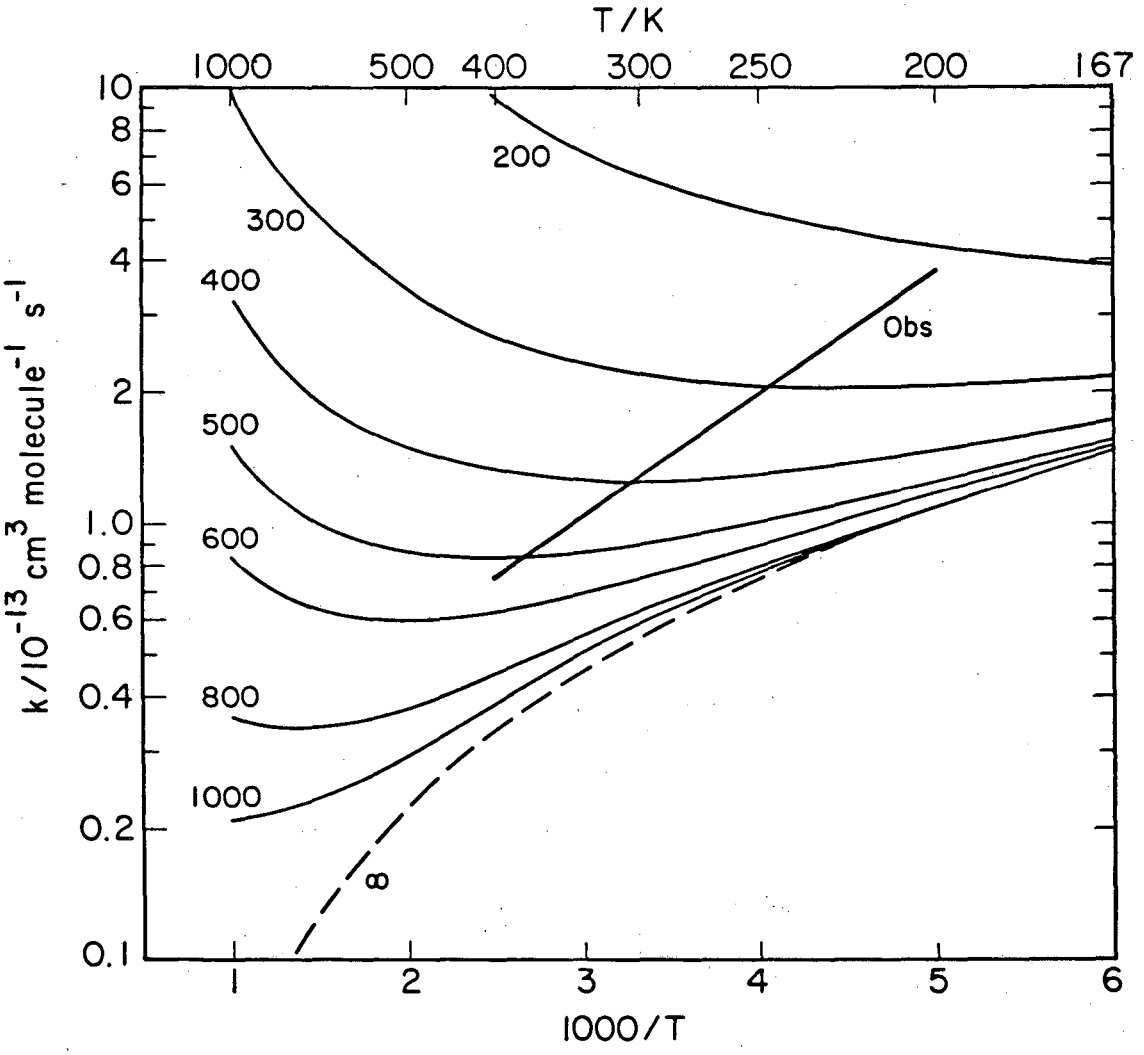
T/K
1000
500
400
300
250
200
167
10
8
6
4
2
1.0
0.8
0.6
0.4
0.2
0.1
200
300
400
500
600
800
1000
∞
Obs
k/10^-13 cm^3 molecule^-1 s^-1
1
2
3
4
5
6
1000/T

Fig. 9

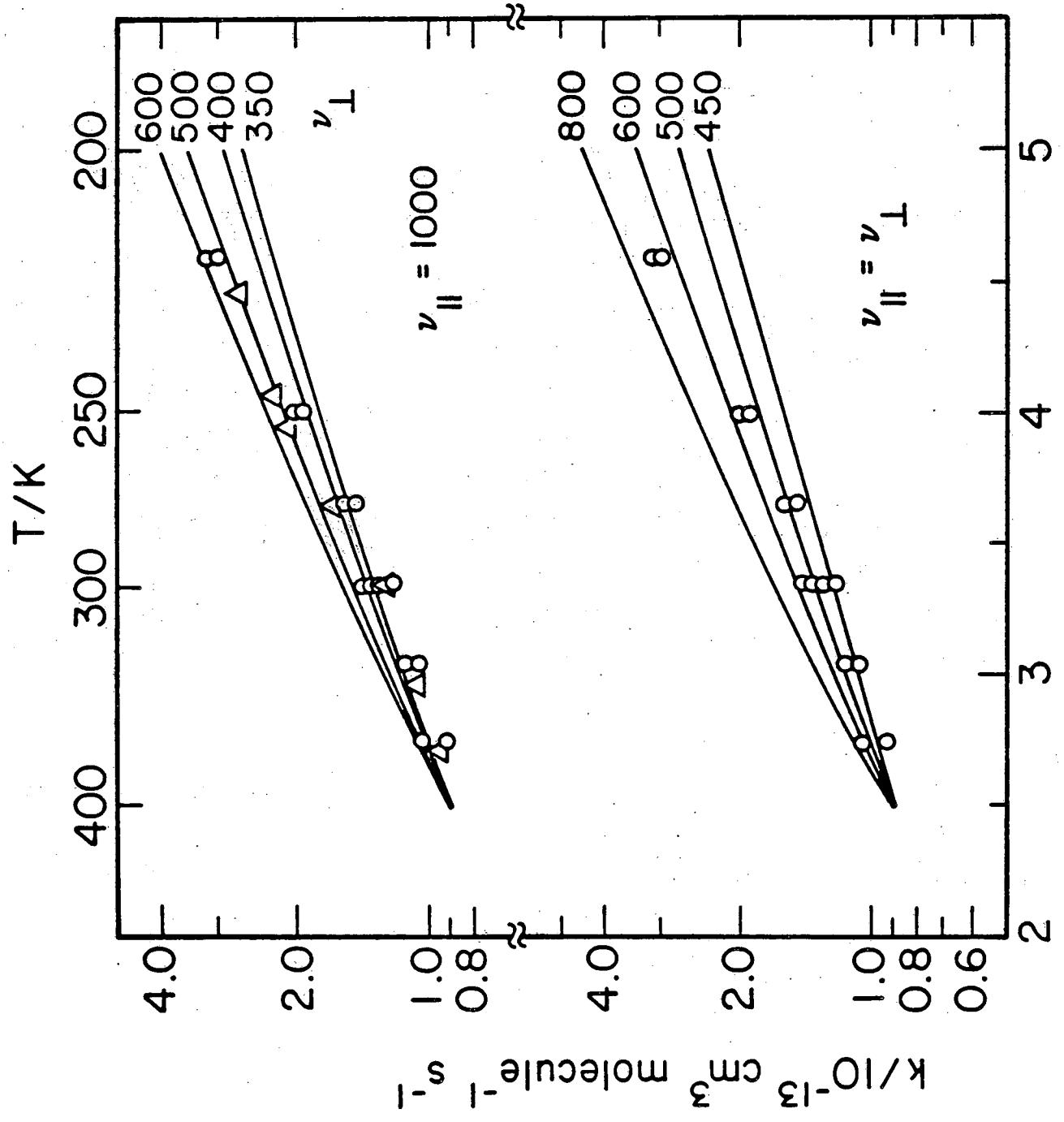
T/K
400
300
250
200
1000/T
5
4
3
2
$k/10^{-13}$ cm$^3$ molecule$^{-1}$ s$^{-1}$
4.0
2.0
1.0
0.8
0.6
$\nu_{\parallel} = 1000$
$\nu_{\perp}$
600
500
400
350
$\nu_{\parallel} = \nu_{\perp}$
800
600
500
450

Fig. 10

This report was done with support from the Department of Energy. Any conclusions or opinions expressed in this report represent solely those of the author(s) and not necessarily those of The Regents of the University of California, the Lawrence Berkeley Laboratory or the Department of Energy.

Reference to a company or product name does not imply approval or recommendation of the product by the University of California or the U.S. Department of Energy to the exclusion of others that may be suitable.

*TECHNICAL INFORMATION DEPARTMENT*
*LAWRENCE BERKELEY LABORATORY*
*UNIVERSITY OF CALIFORNIA*
*BERKELEY, CALIFORNIA 94720*